Insights on the origin of oldhamite in enstatite meteorites from Ca stable isotopes

Wei Dai, Frederic Moynier, Julien Siebert

Insights on the origin of oldhamite in enstatites meteorites from Ca stable isotopes

Wei Dai[1,*], Frederic Moynier[1], Julien Siebert[1]

[1] *Universite Paris Cité, Institut de Physique du Globe de Paris, CNRS, 1 rue Jussieu, Paris 75005, France*

***Corresponding author:** Wei Dai, dai@ipgp.fr

Abstract

In order to understand the origin of oldhamite (CaS) in enstatite meteorites, we report Ca isotopic compositions ($\delta^{44/40}$Ca) of oldhamite (obtained from water leachate of bulk chondrites and aubrites and mineral separates from the Norton County aubrite) and silicate minerals from different types of enstatite chondrites and aubrite. The $\delta^{44/40}$Ca of the bulk enstatite chondrites range from 1.05‰ to 1.24‰, with an average of 1.13±0.12‰, higher than that of the estimate of the bulk silicate earth (~0.94‰). Major and trace element analyses show that the water leachates of enstatite chondrites are mainly composed of oldhamite, and they take over 20.6-68.5% Ca of the bulk meteorite Ca budget. The Ca isotope fractionation between oldhamite and residual silicate ($\Delta^{44/40}Ca_{oldhamite\text{-}silicate}$) for the studied enstatite chondrites is minimum (-0.44‰) for Abee (impact-melt breccia) and maximum (+0.16) for St.Marks (EH5). The Ca isotope fractionation between oldhamite (individual mineral grains and leachate) and silicates in Norton County varies from -0.47‰ to -0.31‰ with an average of -0.41‰. These $\Delta^{44/40}Ca_{oldhamite\text{-}silicate}$ correlate well with previous theoretical calculation and suggests that the oldhamites in Norton County are in isotopic equilibrium with co-existing silicates, and therefore were formed during magmatic processes. However, in enstatite chondrites, the large variation on $\Delta^{44/40}Ca_{oldhamite\text{-}silicate}$ and its negative correlation with metamorphic temperature reflects the redistribution and equilibration of Ca isotopes during metamorphism. The variable $\Delta^{44/40}Ca_{oldhamite\text{-}silicate}$ found in unequilibrated chondrites reflect kinetic Ca isotope fractionation between oldhamite and nebular gas and therefore is evidence for the formation of oldhamite by condensation in the solar nebula.

Key words: Oldhamite, Enstatite chondrite, Ca isotope

1 Introduction

Enstatite meteorites (both chondrites and achondrites) play a special role in planetary sciences as they possibly share a genetic link with the materials that have formed the Earth (Javoy, 1995; Javoy et al., 2010). This is because they are the only meteorites displaying isotope similarities with Earth for many elements, such as O, N (Javoy et al., 1986), Ca (Schiller et al., 2018; Valdes et al., 2014), Ti (Trinquier et al., 2009; Zhang et al., 2012), Nd (Boyet and Carlson, 2007) or Cr (Mougel et al., 2018). However, enstatite meteorites and the Earth have distinct chemical composition, Si isotopic composition and redox state that are difficult to reconcile with a simple common origin (e.g., Fitoussi and Bourdon, 2012). Unlike most other types of meteorites and rocky planets, enstatite chondrites formed under highly reducing conditions (5 log units below the iron-w*ü*stite buffer, $\Delta IW < -5$). Under these particular conditions, elements that are usually considered lithophile under the Earth mantle conditions tend to be siderophile and/or chalcophile (Gannoun et al., 2011; Lodders and Fegley, 1993). This is attested by the presence of various unusual sulfide phases in these rocks (Keil, 1989; Mason, 1966). Among these sulfides, oldhamites, CaS, has attracted much attention for their enrichment in rare-earth element (REE) and potentially control the REE and Ca budget of these meteorites.

The stability of oldhamites in enstatite meteorites is strongly influenced by factors such as oxygen fugacity and saturation of relative elements. As a result, oldhamite have the potential to serve as a tracer for understanding the formation and evolution history of enstatite meteorites. However, the origin of oldhamites in enstatite meteorites remains a subject of debate. It has been proposed that oldhamites are direct condensates from the solar nebula based on their high concentrations of REE (e.g., 10 to 100 times the mean CI chondrite abundance; Gannoun et al., 2011; Lodders and Fegley, 1993). On the other hand, observations of REE enrichments in oldhamites within enstatite achondrites (aubrites) is puzzling, as oldhamite formed during the aubrite melting episode should not be REE-rich for its low partition coefficients relative to silicate melt (McCoy et al., 1999). This discrepancy has led to alternative explanations such as magmatic origin for CaS crystallizing from an evolved melt depleted in FeO and enriched in incompatible

elements (Wood et al., 2014). Furthermore, the REE patterns in oldhamites are highly variable, even within the same meteorite specimen. This suggests that various oldhamite minerals may have different origins (Gannoun et al., 2011). Despite conducting detailed physicochemical or experimental modeling, no direct evidence has been provided to definitely confirm the origin of oldhamites in enstatite meteorites.

Calcium (Ca) has 6 stable isotopes, ^{40}Ca (96.94 %), ^{42}Ca (0.647 %), ^{43}Ca (0.135 %), ^{44}Ca (2.086 %), ^{46}Ca (0.004 %) and ^{48}Ca (0.187 %), with ^{40}Ca a major product of the decay of ^{40}K ($T_{1/2}$=1.25 Ga) and other isotopes formed by various nucleosynthetic mechanisms. It makes Ca isotopes a powerful tool on tracing planetary formation and evolution by studying the stable isotopic variations, the radiogenic enrichment for age dating and nucleosynthetic anomalies (Russell et al., 1978; Schiller et al., 2018; Yokoyama et al., 2017). Several studies have provided Ca isotope composition on enstatite meteorites with a discrepancy between different laboratories (Huang and Jacobsen, 2017; Simon and DePaolo, 2010; Valdes et al., 2014). This variability in Ca isotopic compositions could be attributed to two potential factors: the heterogeneity in proportion of Ca-dominant minerals or preferential dissolution of oldhamite (Valdes et al., 2014). Theoretical ab-initio calculations have suggested that oldhamite minerals should exhibit enrichment in lighter Ca isotopes compared to a silicate melt during magmatic processes (Huang et al., 2019). However, the actual Ca isotope composition of oldhamite in enstatite meteorites remains poorly constrained due to limited data. To date, only one study has determined the Ca isotope composition of oldhamite in an EH4 enstatite chondrite. Surprisingly, the study found that oldhamite in this particular meteorite is isotopically heavier than co-existing silicate minerals by leaching oldhamite from bulk rock in water (Valdes et al., 2014). This is opposite to theoretical calculation which implies that the origin of oldhamites could be more complex than initially expected.

In order to trace the origin of oldhamite in enstatite meteorites and further explore their relationship with Ca isotopic variation among enstatite meteorites, we have carefully selected different types of enstatite chondrites and achondrites for analysis. The enstatite chondrites chosen to encompass varying degrees of metamorphism grades, from EH3 to EH6 and one EH-type impact breccia, along with one EL3 and three EL6 samples. As a representative of igneous achondrite we have included the aubrite sample, Norton County, which is known for containing large size oldhamite phenocrysts.

Previous study has attempted to extract oldhamite from bulk meteorite powder with water, considering its water solubility while other Ca-bearing minerals remain in silicate form. However, these studies have not provided the major element composition of the leachates, which has made it challenging to validate the efficiency of oldhamite extraction (Valdes et al., 2014). In this study, we also adopt the water leaching to extract oldhamite and report the Ca isotopic compositions ($\delta^{44/40}$Ca) of the leachate (oldhamite) and remaining portion (silicates). This will enable us to gain valuable insights into the isotopic variations and better understand the role of oldhamite in Ca isotope variations among enstatite meteorites. To further validate the efficiency of our water leaching experiments, we have selected two individual oldhamite phenocrysts from the aubrite sample, Norton County, for a direct comparison. This comparative analysis will help us assess the consistency and reliability of our extraction method.

By conducting a thorough investigation with these diverse enstatite meteorite samples, we aim to understand oldhamite's origin and its contribution to Ca isotopic variation. This research will shed light on the processes involved in the formation and evolution of oldhamite in enstatite meteorites.

2 Sample and analytical method

2.1 Sample description and leaching experiments

For our study, we have carefully chosen a diverse set of meteorite samples. This includes seven EH-type (Qingzhen (EH3), Sahara 97096 (EH3), NWA13299 (EH3), Indarch (EH4), St. Marks (EH5), NWA12945 (EH6)), one EH-type impact-melt breccia (Abee (IMB)) and four EL-type (MAC02837 (EL3), Ufana (EL6), Pillistfer (EL6), Hvittis (EL6)) enstatite chondrites. Moreover, a single aubrite, Norton County, has been included for this study. The enstatite chondrites chosen for analysis display a range of metamorphic grades, spanning from 3 to 6. The bulk rock Ca isotope composition of several samples, including Qingzhen, Sahara 97096, Abee, Indarch, St. Marks and Norton County, have been previously reported in the literature (Huang and Jacobsen, 2017; Simon and DePaolo, 2010; Valdes et al., 2014). Notably, a previous study has examined the oldhamite in Indarch using water leaching experiment (Valdes et al., 2014). In this study, we have extended the research by reporting the Ca isotope composition of both bulk

meteorite samples and water leachate along with their residues. Furthermore, we have isolated and analyzed two individual oldhamite mineral phenocrysts (>80 mg) from the Norton County aubrite. The chemical composition and Ca isotope composition of these phenocrysts will be used for direct comparison with the result obtained from the water leaching experiments. As part of our analytical framework, we have utilized a USGS (United States Geological Survey) reference material (GSP-2) and a seawater standard (NASS-7). These reference materials were digested, purified and analysed alongside our meteorite samples, ensuring accuracy and precision in our measurements.

To prepare the samples for analysis fresh rocks pieces were crushed into powders without using water cleaning. Although grain size of the powder could not be determined, we checked by eyesight for the absence of residual coarse grains or metal nodules after crushing. The resulting bulk rock powder samples (~15 mg) were dissolved using a mixture of 1 ml concentrated HNO_3 + 1 ml concentrated HF in 7 ml Teflon bomb vessels. This dissolution process took place in an oven (120°C) for 2 days (Inglis et al., 2018). After evaporation of the HF and HNO_3, the samples underwent further treatment. A 1:1 volume mix of concentrated HNO_3 and HCl was used to treat the samples, which were refluxed in the oven at 135°C for a duration of 3 days. Finally, the samples were dried and redissolved in 4 mol/L HNO_3 for chemical purification.

In order to investigate the role of oldhamite on element abundances and isotopic composition in the whole rock budget, we conducted a series of leaching experiments. The experimental procedure involved the following steps:

1. Sample preparation: approximatively 20 mg samples were carefully weighted and placed in small pre-cleaned tubes.
2. Leaching process: We added 1 ml MQ water to the tubes containing the samples and agitated them for several minutes. This agitation promoted the reaction between oldhamite and water. Then the liquid was extracted following centrifugation. This leaching process was repeated for 2-3 times to ensure thorough separation of oldhamites.
3. Conversion to $Ca(NO_3)_2$: The leached fraction was then treated with 1ml of concentrated HNO_3 (~69 %) which converted all the Ca present into $Ca(NO_3)_2$ and then the samples were dried down.
4. Ca purification: To prepare the samples for Ca purification, 1 mL of 4 mol/L HNO_3 was added and ion exchange chromatography was employed.

Additionally, we conducted separate digestion of single oldhamite mineral separates obtained from Norton County aubrite using the same process as the leachates. The remaining portion of the leaching experiments, known as residues, were transferred to Teflon vessels. These residues were digested using the same procedure as bulk rock powders.

2.2 Chemical purification

Before proceeding with the Ca isotope purification process, we separated 5% (50 μL) of each solution fraction, which was then diluted in 5 mL 0.5 mol/L HNO_3 for major and trace element analysis. The remaining solutions were further diluted with 4 mol/l HNO_3 to achieve a Ca concentration of about 10 μg/g Ca in the solution before loading the samples. For chemical separation, we employed a well-documented procedure that has been used in previous studies (Dai et al., 2022), originally adapted from Valdes et al. (2014) by Feng et al. (2018). Here we provide a concise summary of the process. The chemical purification was conducted using a column filled with 250 μL of Eichrom DGA resin. After washing the columns, the samples were loaded in 0.4 mL of 4 mol/L HNO_3, which contain ~4 μg of Ca. The matrix elements were washed by adding 6.75 mL of 4 mol/L HNO_3, and the Ca fraction was collected with 3 mL of water. This procedure was performed twice to ensure thorough purification. Next, to eliminate Sr interference, the Ca fraction was further purified by passing it through ~100 μL of Eichrom Sr spec resin. After washing the resin, the samples were loaded in 0.5 mL of 3 mol/L HNO_3, and the calcium was collected with an additional 1.5 mL of 3 mol/L HNO_3. This collected Ca fraction was then dried down at 120°C. Several drops of concentrated HNO_3 were added and evaporated to decompose potential organic matters leached during the column chemistry. Full procedural blanks were tested and was below ~3.4 ng, consistent with previous studies done at IPGP (Valdes et al., 2014). Finally, the samples were redissolved in 0.5 mol/L HNO_3 for analysis on the multiple-collector inductively-coupled-plasma mass-spectrometry (MC-ICP-MS), Nu Sapphire.

2.3 Calcium isotope measurement on the Nu Sapphire

The detailed information for Ca isotope measurement on Nu Sapphire has been already documented (Dai et al., 2022). In this study, we report the mass-dependent deviation and the radiogenic Ca anomaly at the same time. For mass-dependent deviation, the data are originally

reported as $\delta^{x/44}Ca$:

$$\delta^{x/44}Ca=\left(\frac{(^{x}Ca/^{44}Ca)_{sample}}{(^{x}Ca/^{44}Ca)_{SRM915b}}-1\right)\times 10^{3}$$

With x=40, 42, or 43. While the radiogenic input on ^{40}Ca is reported using the epsilon notation as:

$$\varepsilon^{40}Ca=\left(\frac{(^{40}Ca/^{44}Ca)_{n\ sample}}{(^{40}Ca/^{44}Ca)_{n\ SRM915b}}-1\right)\times 10^{4}$$

With $(^{40}Ca/^{44}Ca)_n$ representing the $^{40}Ca/^{44}Ca$ ratio corrected from the mass-dependent isotopic fractionation after being normalized to the $^{42}Ca/^{44}Ca$ ratio using the exponential law and a $^{42}Ca/^{44}Ca$ ratio of 0.31221 (Russell et al., 1978). Changes in the abundance of ^{40}Ca relative to other calcium isotopes can originate from nucleosynthetic anomalies, as well as from the radioactive decay of ^{40}K to ^{40}Ca by electron ($\beta-$) emission (half-live of 1.27 billion years). Due to higher K/Ca ratios in some chondrites, radioactive decay can produce up to 4.02 ε-unit increase in ^{40}Ca over the age of the Solar System. The initial $\varepsilon^{40}Ca$ values, which reflect the nucleosynthesis anomalies, were reported as $\varepsilon^{40}Ca_0$ after correction of the radioactive decay of ^{40}K using the age of the samples. The effect of concentration mismatch on Sapphire is more significant than on other MC-ICP-MS and such effect could be variable due to the modification of tuning parameter at the beginning of each session. To avoid the concentration mismatch effect, a simple calibration was performed based on the method described in Dai et al. (2023a).

In this study, all the data have been acquired using SRM 915b as the standard because the original SRM 915a standard is not commercially available anymore. To facilitate comparison with previous data we have renormalized to SRM 915a and present the stable isotope data as $\delta^{44/40}Ca$ as used in most studies (Antonelli et al., 2019; Huang and Jacobsen, 2017; Simon et al., 2009).

The long-term external reproducibility was determined by the analysis of reference material GSP-2 and NASS-7 on Sapphire over an eleven-month period (Dai et al., 2023b). The external reproducibility of $\delta^{44/40}Ca$ and $\varepsilon^{40}Ca$ are 0.07 ‰ and 0.50 ε-unit (2SD), respectively, typically better than what was obtained on thermal ionization mass spectrometry (TIMS) and older generation of MC-ICP-MS (>0.10‰, 2SD). The $\delta^{44/40}Ca$ values of NASS-7 and GSP-2 are 1.92 ± 0.08 ‰ (2SD) and 0.71 ± 0.08‰ (2SD), while their $\varepsilon^{40}Ca$ values are -0.16 ± 0.27 ‰ (2SE) and 4.36 ± 0.49‰ (2SE), respectively, consistent with literature values (Amsellem et al., 2017; Feng et al., 2018; He et al., 2017; Li et al., 2018; Liu et al., 2017; Schiller et al., 2012; Valdes et al., 2014).

3 Results

The Ca isotope data for the oldhamite leachates, silicate residues and bulk rocks of enstatites are listed in Table 1 and presented in Figure 1. The $\delta^{44/40}$Ca of the bulk EH chondrites range from 1.05 ± 0.07‰ to 1.15 ± 0.04‰, with an average of 1.10 ± 0.06‰ (2SD, n=7). The EL3 chondrite displays identical $\delta^{44/40}$Ca value with EH chondrites. In contrast, the $\delta^{44/40}$Ca values of the bulk EL6 chondrites are higher than other samples, with an average of 1.22 ± 0.03‰ (2SD, n=3). The aubrite, Norton County, show similar $\delta^{44/40}$Ca values (1.12 ± 0.05‰) to enstatite chondrites. These findings suggest that the $\delta^{44/40}$Ca of enstatite chondrites is higher than that of bulk silicate Earth (~0.94‰). The Ca isotope fractionation between oldhamite and residual silicate part is reported as $\Delta^{44/40}Ca_{oldhamite\text{-}silicate} = \delta^{44/40}Ca_{leachate} - \delta^{44/40}Ca_{residue}$. The values of $\Delta^{44/40}Ca_{oldhamite\text{-}silicate}$ vary across different chondrites and generally correlate with the metamorphic grade of each sample. For instance, Abee (IMB) exhibits a $\Delta^{44/40}Ca_{oldhamite\text{-}silicate}$ of -0.44‰, while St Marks (EH5) displays a value of +0.16‰. Norton County's $\Delta^{44/40}Ca_{oldhamite\text{-}silicate}$ is determined to be -0.31 ± 0.09‰ while the difference between individual oldhamite grains within Norton County is found to be -0.44 ± 0.08‰ and -0.47 ± 0.08‰, respectively.

The abundance of radiogenic ^{40}Ca (produced by the radioactive decay of ^{40}K), in the analyzed fractions (bulk rocks and leachates containing oldhamites and residues) varies with different K/Ca ratios. To determine the initial ε^{40}Ca values of different enstatites, we calculated the average values from the bulk, leachate and residual parts. The initial ε^{40}Ca values span a range from -0.81 to +0.41, with an average of -0.36 ± 0.23 (2SE). These results are consistent with the ε^{40}Ca values of the bulk silicate earth.

The water solubility of alkali sulfides, such as oldhamite and niningerite, leads to the preferential extraction of these minerals in water leachates, while silicates, metals, and other sulfides (e.g., FeS) remain in the residual material. Consequently, this leaching process effectively separates the calcium (Ca) present in oldhamites and other silicate phases. The mass and elemental budgets of leachates are computed and presented in Table 2. Due to the unknown exact mass of leachates and residues, the mass fraction of leachates is determined by assuming that all the leached components consist of sulfides and by dividing the weight of leachates to the weight of

the bulk rock powder before leaching (see Table S1). Similarly, the relative elemental budget is obtained using the same methodology. Throughout our analysis, we observed that the leachates mainly consist of Ca, with limited amounts of Mg, Na, Mn and Fe (Figure 2). The analysis indicates that the leached minerals are predominantly composed of oldhamite, with some presence of niningerite and a NaS-rich phase. It is noteworthy that the abundance of the NaS-rich phase decreases as the metamorphic grade advances, especially in EH chondrites. The mineral proportion of oldhamite within the leachates varies, ranging from 0.3% to 2.0%. This represents a significant portion, accounting for 20.6% to 68.5% of the Ca budget, overall agree with the efficiency on extracting oldhamites by using water or weak acetic acid in literatures (Boyet and Gannoun, 2013).

The REE pattern and budget indicate that the leachates contain 0.7% to 8.2% of the REEs (based on Ce as an example), compared to the bulk rock. Considering the proportion of leached minerals in the bulk rock, the leachates have CI-normalized REE concentrations ranging between 1 and 10, lower than that from literatures (e.g., 10 to 100 times the mean CI chondrite abundance; Gannoun et al., 2011; Lodders and Fegley, 1993). However, two individual oldhamite grains exhibit significantly high concentrations of REEs, reaching approximately 100 times the mean CI chondrite abundance. Regarding the REE patterns, the leachates from EH-type chondrites exhibit nearly flat patterns, while those from EL-type and aubrite samples show negative Eu anomalies.

4 Discussion

4.1 Calcium isotope composition of enstatite chondrites

Previous studies suggested the enstatite meteorites could be the potential source for rocky planets like Earth, attributed to their similar isotopic compositions (Javoy et al., 2010). However, the significant variation in the $\delta^{44/40}$Ca values among enstatite meteorite samples, ranging from 0.95‰ to 1.46‰, and even exhibiting variability within the same sample have been used to argue for such an enstatite chondrites/Earth connection (Amsellem et al., 2017; Huang and Jacobsen, 2017; Simon and DePaolo, 2010; Valdes et al., 2014). Here we find that the $\delta^{44/40}$Ca values of the bulk rocks are remarkably consistent, with an average of 1.13 ± 0.12‰ (2SD, N = 11). This finding deviates from the existing literature data and underscores the need for a more

comprehensive discussion regarding the factors contributing to the observed variation. The precise determination and constraint of the average $\delta^{44/40}$Ca of enstatite chondrites are crucial to gain a better understanding of their isotopic composition and its potential implications for the formation of rocky planets.

Sample heterogeneity provides a plausible explanation for the observed variations. In the case of enstatite meteorites, the amount of oldhamites is relatively minor (<1%) but it significantly contributes to the bulk rock's Ca content (20.6% to 68.5% in this study). It is worth noting that oldhamites are soluble in water and susceptible to degradation under oxidizing conditions. Consequently, their loss during alteration processes on Earth's surface or even during sample cleaning procedures, as proposed by Valdes et al. (2014), could account for the discrepancies in isotopic composition compared to the findings by Simon and DePaolo (2010).

Here, we focus on Ca isotope data for the Abee (IMB) meteorite (Figure 3) to evidence this. Previous studies have reported a range of $\delta^{44/40}$Ca values for Abee, spanning from 0.95‰ to 1.34‰, while our data falls well within this range (1.11 ± 0.05‰, 2SD). It is noteworthy that the oldhamite leachate and silicate component of Abee align coincidentally with the $\delta^{44/40}$Ca variation observed in the bulk rock across different literature sources. By conducting a modal calculation of the calcium budget for an average enstatite material, approximately 50% of the calcium is contained within oldhamites (Piani et al., 2016). In this study, the measured $\delta^{44/40}$Ca values of enstatite chondrites and the calculated $\delta^{44/40}$Ca values derived from a mass-balance calcium budget exhibit excellent agreement. This indicates that the samples analyzed in this study are homogeneous.

Furthermore, the $\delta^{44/40}$Ca values of bulk EL6 chondrites range from 1.16‰ to 1.24‰, slightly higher than those of other enstatite chondrites. The elevated $\delta^{44/40}$Ca values observed in EL6 chondrites could be attributed to calcium loss resulting from the extraction of metals or sulfides during metamorphism. Unlike EH chondrites, EL chondrites exhibit lower abundances of metal and sulfide phases, larger chondrule sizes, and depletion of least refractory rare earth elements (REEs) such as Eu and Yb (Barrat et al., 2014). These characteristics are explained by a potential early melting event that occurred prior to the accretion of the final parent body (Horstmann et al., 2014; Weyrauch et al., 2018). Although oldhamite has a high melting temperature as a pure substance (2450-2525°C, Chase and Organization, 1998), it can easily melt

and dissolve in silicate melts at high temperatures. Experimental results have confirmed that all metal-sulfide components completely melt at 1000°C when the EH4 chondrite Indarch is heated in a closed system (Fogel et al., 1996; McCoy et al., 1999). Consequently, the extraction of a plagioclase and oldhamite-bearing melt has been proposed to explain the observed calcium depletion observed in EL6 chondrites (Rubin et al., 2009). Interestingly, the oldhamites in EL6 chondrites exhibit lower $\delta^{44/40}$Ca values than the co-existing silicate fraction, suggesting that the loss of this mineral may contribute to the heavier $\delta^{44/40}$Ca values observed in EL6 chondrites compared to other enstatite chondrites. Except for the EL6 chondrites with Ca loss by later events, the average $\delta^{44/40}$Ca value of EH and EL3 chondrites (1.10 ± 0.06‰, 2SD) provided herein represents the most precise estimate to date for enstatite chondrites.

4.2 Oldhamites in Norton County: igneous origin

The origin of oldhamites in aubrites, which are suggested to be igneous rocks from differentiated planetary bodies, continue to be a subject of debate regarding their nebular or magmatic origins (Floss and Crozaz, 1993; Lodders, 1996; Wheelock et al., 1994). The uncertainty arises from their rare earth element (REE) abundances and complex REE patterns, which do not align with sulfide/silicate melt REE partition coefficients derived from experimental studies (Dickinson and McCoy, 1997; Floss and Crozaz, 1993). In this study, the Ca composition of oldhamite individual grains, leachate fraction and silicate parts provide valuable insights into the origins of oldhamite in aubrites, thereby contributing to the ongoing discussion surrounding their formation mechanisms.

Both individual oldhamite grains and leachate fractions exhibit a negative europium (Eu) anomaly (Figure S1), similar to oldhamite grains found in igneous contacts with other aubritic minerals reported in the literature (Wheelock et al., 1994). The $\delta^{44/40}$Ca value of the silicate fraction is determined to be 1.27 ± 0.08‰, while the leachate fraction displays a lower value of 0.96 ± 0.06‰. The two individual oldhamite grains exhibit slightly lower $\delta^{44/40}$Ca values compared to the leachate (0.83 ± 0.03‰ and 0.80 ± 0.05‰ vs 0.96 ± 0.06‰). Huang et al. (2019) conducted calculations on the equilibrium calcium isotope fractionation factor between oldhamite and various silicate minerals, suggesting that oldhamite tends to be enriched in light Ca isotopes compared to silicate minerals. For Norton County, the equilibrium temperature can be estimated

based on its mineral composition. Both the MnS-FeS-oldhamite and Si-kamacite geothermometers provide consistent temperatures around 1130 ± 80 K (Jordan et al., 2019; Lodders, 1996). Under these conditions, the theoretical equilibrium Ca isotope fractionation between oldhamite and different silicate minerals (-0.60‰ to -0.35‰) is consistent with difference observed between the oldhamite and silicate fraction (-0.47 ± 0.08‰ to -0.31 ± 0.09‰), indicating that the oldhamites in Norton County probably are in isotopic equilibrium with co-existing silicates (Figure 4).

The relative enrichment of REEs that we observe in the oldhamites does not match the sulfide/silicate melt REE partition coefficients obtained from experimental studies, where values are typically 1 or less (Dickinson and McCoy, 1997; Ingrao et al., 2019; Lodders, 1996). This discrepancy suggests that the formation of oldhamites is not simply governed by oldhamite/silicate melt equilibrium. An early crystallization of enstatites has been proposed as a mechanism to concentrate REEs in the residual melts, primarily composed of sulfides and albite-like components, and oldhamites could be the final product in such process.

To further explore this phenomenon, a simplified model using the bulk composition of Norton County as the starting material has been used (Figure 5 and Table S2). Assuming the bulk Norton County as initial melt and following a roughly crystallization step by literature (Okada et al., 1988), approximately 95% to 99% silicate crystallization (mainly enstatite and olivine, with limited clinopyroxene and plagioclase) can result in an enrichment of REEs by a factor of 10 to 100 in the residual melt, which agrees with what we observe in the natural samples. Though such magmatic process could start at much higher temperature, the relative low cooling rate of Norton County (1-10 K/Ma) would promote the chemical and isotopic equilibrium at lower temperature which relative to the prior of oldhamite formation (e.g., Okada et al., 1988). Considering the final equilibrium temperature at 1130K, the calculated oldhamites exhibit lower $\delta^{44/40}$Ca values (ranging from 0.91‰ to 0.85‰) than silicate mineral crystallization and are consistent with our observations (0.96‰ to 0.80‰). Our result implies that the oldhamites in Norton County were formed during magmatic processes.

The REE patterns of oldhamites in other aubrites are highly variable, with both positive and negative Eu anomalies, indicating a more complex history. Previous studies suggested that the oldhamites with negative Eu anomalies might be attributed to igneous processing or subsolidus equilibration similar to EL6 chondrites. Meanwhile, some oldhamites in aubrites with positive Eu

anomalies are only observed in EH3-4 chondrites and are suggested to be relict after the formation of aubrite parent bodies (Floss and Crozaz, 1993). The successful application of our approach to Norton County indicates that calcium isotopes are a powerful tool for tracing the origin of oldhamite minerals. However, further studies are required to fully explore this potential and unravel the complexities associated with oldhamite formation in other aubrites.

4.3 Redistribution of Ca isotopes during heating processes on enstatite parent bodies

The Ca isotope fractionation between oldhamite and silicate, $\Delta^{44/40}Ca_{oldhamite\text{-}silicate}$, in enstatite chondrites exhibit variable values from -0.44‰ to +0.16‰, which differs from the result observed in the Norton County aubrite. This suggests that the Ca isotopic variations between oldhamites and the residual fractions does not arise purely from equilibrium Ca isotope fractionation but rather reflects the influence of another process.

Enstatite chondrites have been proposed to undergo subsequent thermal metamorphism induced by the decay of short-lived radionuclides or impacts after their accretion. During this progressive thermal metamorphism from petrologic types 3-6, both the texture and mineralogy of the chondrites have been reset. For instance, the well-defined chondrules present in type 3 chondrites become recrystallized in higher metamorphic grades and even absent in type 6 chondrites. Additionally, the size of crystalline plagioclase increases, while other minerals such as olivine may be absent in high-grade samples (Huss and Lewis, 1994; Huss et al., 2006). For impact-induced breccias, melted chondrules and metal/sulfide-rich shock veins are often observed which indicates that they could be partly melted and recrystallized (Rubin and Scott, 1997).

The heating event accompanying with recrystallization of minerals leads to the redistribution of elements and isotopes, and the metamorphic temperature can be recorded by specific minerals. This is also reflected in the composition of our leachates. As the EH chondrites progress from type 3 to type 6, the Na content in the leachates decreases, suggesting the transfer of Na from sulfide phases to silicate phases or its loss with the extracted melts (Figure 2c). Meanwhile, trace elements, like REEs, U and Th, tend to concentrate in sulfides (Barrat et al., 2023). Various mineral thermometers have been employed to constrain the metamorphic temperature (Zhang and Sears, 1996). Overall, with the progress of metamorphic grade, the relative metamorphic

temperature will also increase (Table S4). For type3 chondrites, the peak temperatures during heating event are lower than 500℃ while for type 5-6 chondrites, such as EH6 and EL6, their peak temperature could reach higher than 800℃ (Huss et al., 2006). The temperature during high grade metamorphism can cause melting and migration of sulfide-rich melts and further improve the chemical and isotopic redistribution between different phases (Fogel et al., 1996; McCoy et al., 1999). The IMB sample Abee shows the lowest $\Delta^{44/40}Ca_{oldhamite\text{-}silicate}$ value among all the enstatite chondrites which is consistent with the value in the igneous aubrite Norton County. It has the highest metamorphic temperature among all the chondrites which is induced by impact event. Such event may have heated them to temperatures higher than their normal metamorphic temperatures after which they were partly molten and rapidly quenched as breccias (Rubin and Scott, 1997). It is worth noting that in some samples like the EH5 St. Marks, the metamorphic temperature does not match their metamorphic grade determined by the morphology. It indicates that the metamorphic events on enstatite chondrites could be complex with multiple stages. Previous studies suggest that EH and EL type chondrites could experience different thermal history on their parent body. For example, Hammouda et al. (2022) proposed that all the EL chondrites may experience a melting event on its parent body due to their identical REE patterns in CaS, while the variation on REE patterns in CaS among EH chondrites should reflect oldhamite recrystallization during metamorphism. In this study, for both EH and EL chondrites, their $\Delta^{44/40}Ca_{oldhamite\text{-}silicate}$ show good correlation with their metamorphic temperature which overall increase from type 3 to type 6 (Figure 4 and S2). The positive $\Delta^{44/40}Ca_{oldhamite\text{-}silicate}$ values are mostly observed in type 3 chondrites with lower metamorphic temperature. Meanwhile, the samples with higher metamorphic temperature have much lower $\Delta^{44/40}Ca_{oldhamite\text{-}silicate}$ values and the oldhamite and silicate phases tend to reach Ca isotopic equilibrium. This trend clearly indicates a process of Ca redistribution from the least equilibrated type 3 chondrites to the near Ca isotopic equilibrium observed in type 6 chondrites, driven by heating metamorphism and widely occurs in both EH and EL chondrites.

4.4 Condensation origin of oldhamite in unequilibrated EH3 chondrites

During heating metamorphism, the redistribution of Ca isotopes is common as discussed above. It is noteworthy that for EH3 chondrites, all the oldhamite leachates exhibit higher $\delta^{44/40}Ca$

values compared to the co-existing silicates, and they plot the farthest from the metamorphic re-equilibrium trend. EH3 chondrites are the least affected by metamorphism, and thus potentially preserving nebular isotopic and chemical characteristics.

A model for the early evolution of the enstatite chondrite parent bodies is an onion-shell-layered structure, with type 3 chondrites representing the surface layer that experienced the least metamorphic effects (Trieloff et al., 2003). In the context of chondrite metamorphism, the maximum heating temperatures estimated for EH3 chondrites are estimated to be lower than 500 ℃, as indicated by thermometers such as Fe-Ni-P and niningerite-alabandite (Huss et al., 2006; Zhang and Sears, 1996). In contrast, the temperature estimates derived from oldhamite suggest temperatures of 700-800 ℃, which are significantly higher than the peak temperature of the metamorphism (Table 2 and Figure S2) and higher than the metamorphism temperatures defined for EH4-6. This observation suggests that the temperatures recorded by oldhamites may represent other events that occurred before accretion, rather than being indicative of heating metamorphism.

In details, at least two distinct groups of oldhamite with different origins have been observed in chondrules and metal-sulfide clasts in EH3 chondrites based on their morphology and REE patterns, suggesting a complex history within the solar nebula (Gannoun et al., 2011). Enstatite chondrites are predominantly composed of chondrules (approximately 80%) with limited matrix. One proposed explanation for the origin of oldhamites is their formation within chondrules. Piani et al. (2016) suggested that oldhamites in chondrules were formed through sequential sulfide saturation during the interaction between chondrule melts and sulfur-rich gases or directly crystallized from the melt. However, if this were the case, no variation on REE patterns should be observed in oldhamites due to the expected oldhamite/silicate melt partition coefficients. Most oldhamites in enstatite chondrites are found in the matrix rather than within chondrules (Weisberg and Kimura, 2012). The leachates obtained from EH3 chondrites using weak acid solutions yield nearly flat CI-normalized REE patterns, which differs from the strong positive anomalies for both Eu and Yb observed in single CaS grains analyzed by in-situ techniques (Barrat et al., 2014). This discrepancy suggests the presence of a sulfide phase with negative Eu and Yb anomalies, which is believed to be concealed within the fine-grained matrix (Hammouda et al., 2022). Assuming the oldhamites grains in chondrules with positive Eu anomalies and significant REE enrichment were

produced during later chondrule formation events (Piani et al., 2016), this "missing" part in matrix should reflect other process which resembles the first condensates from a reduced nebular gas (Ebel et al., 2006; Hammouda et al., 2022). To reconcile the mass balance between leachate and in-situ data, it is proposed that this missing phase, considered as an early condensate material, constitutes over 90% of the leachate, while the rest parts are niningerite grains (5% to 6%) and REE-enriched oldhamites (~1%) (Hammouda et al., 2022). Throughout our mass balance calculation, the leachates from EH3 chondrites consist of 51.6% to 61.7% oldhamites, 19.6% to 26.8% niningerite and 11.5% to 27.2% Na-rich sulfides. As a result, the missing component is likely to be dominated by oldhamite with limited Na, Mg, and K. Consequently, most oldhamites in EH3 chondrites are in matrix and represent the product from solar nebula. The observed positive $\Delta^{44/40}Ca_{oldhamite\text{-}silicate}$ values in unequilibrated EH3 chondrites, which is the farthest from the equilibrium Ca isotope fractionation between oldhamite and silicate minerals, should reflect kinetic Ca isotope fractionation between oldhamite and the nebular gas, providing evidence for the formation of oldhamite through condensation or interaction with the gas in the solar nebula. As previous study suggested, Ca isotopic composition of oldhamites could provide a way to constrain the formation process of enstatite chondrites in the future (Huang et al., 2019).

4.5 Calcium isotope evolution of reduced planet embryos

It is believed that during the early stage of planetary formation the rocky planetary embryos like proto-Earth are more reduced than during the final stages and similar to Mercury (e.g., Wadhwa, 2008; Wohlers and Wood, 2015). Under reducing conditions, Ca and other elements normally regarded as lithophile elements can become siderophile and/or chalcophile, leading potential elemental and isotopic fractionation during differentiation (Anzures et al., 2020; Cartier and Wood, 2019). Some of these elements are thought to sink into core with sulfides like FeS during the magma ocean differentiation (Barrat et al., 2023). The oldhamite with other alkali metal sulfides are often observed to co-exist with troilite in enstatite chondrites. As its density is significantly lower than troilite and other silicate minerals, oldhamites (and other alkali sulfides) should likely separate from FeS melt and migrate to the surface of the planetary embryos (Siebert et al., 2004). During the later global magma ocean stage, these sulfide melts should dissolve in silicate melts and crystalize at the top of the magma ocean eventually to form a primordial

planetary crust (Cartier and Wood, 2019). These crusts would mainly consist of oldhamite and plagioclase which could be the main reservoir of REE and other incompatible elements (Figure 6).

Up to now, the building blocks of Mercury are still debated, but enstatite meteorites (especially aubrites) are considered as the best analogue rocks of Mercury's surface for their similar oxygen fugacity (Cartier and Wood, 2019; Udry et al., 2019). The significant Ca isotope fractionation between oldhamite and silicate phases evidenced in the present work indicates that Ca isotope should fractionate during a mercurial magma ocean differentiation. About 7-11 % of S is suggested to remain in mercury's silicate mantle (Namur et al., 2016), mainly composed of forsterite and enstatite, with minor amounts of clinopyroxene and Ca-Mg-Fe sulfide complex (Cartier and Wood, 2019). The oldhamites, together with graphite and plagioclase should migrate to the surface for their lower density than other minerals during magmatic evolution. This is in agreement with the MESSENGER spacecraft observations showing that Mercury has a Fe-poor and S-rich crust in which sulfur are mainly present as oldhamite and niningerite (Malavergne et al., 2014). The thickness of the mercurial crust is estimated to be about 35-53 km, with a density of about 2.7-3.1 g/cm^3, which represents 2.5% of the total mass of Mercury (mantle 23.5%) (Vander Kaaden and McCubbin, 2015). Assuming that the Norton County aubrite is a relevant analog of Mercury's mantle, silicate cumulates containing enstatite and forsterite with higher $\delta^{44/40}$Ca (1.29-1.40‰) would sink into the deeper mantle leaving a layered crust composed of plagioclase and oldhamite with a lower $\delta^{44/40}$Ca value (0.92-0.98‰) and a 0.4-0.5‰ Ca isotopic difference between mantle and crust (Figure 6).

5 Conclusion

Calcium isotopic compositions ($\delta^{44/40}$Ca) of oldhamite (obtained from water leachates of chondrites and aubrites and separated minerals from the Norton County aubrite) and silicate minerals from enstatite meteorites were measured to study the origin of oldhamites and further discuss their relationship with the Ca isotopic variation observed among enstatite meteorites. The $\delta^{44/40}$Ca of the bulk enstatite chondrites range from 1.05‰ to 1.24‰, with an average of 1.13 ± 0.12‰, which is higher than the estimated value of the bulk silicate Earth (~0.94‰). Except for the EL6 chondrites which suffered Ca loss due to secondary events, the average $\delta^{44/40}$Ca value of

EH and EL3 chondrites (1.10 ± 0.06‰, 2SD) provided in this study is the most precise constrain on the average $\delta^{44/40}$Ca of enstatite chondrites. The Ca isotopic fractionation between oldhamite (individual mineral grains and leachates) and silicates in Norton County varies from -0.47‰ to -0.31‰ with an average of -0.41‰, which is consistent with previous theoretical calculation of equilibrium Ca isotopic fractionation. It suggests that the oldhamites in Norton County were formed at isotopic equilibrium with co-existing silicates. This provides direct evidence that these oldhamites were formed during magmatic processes rather than being inherited from nebular condensation processes. The $\Delta^{44/40}Ca_{oldhamite\text{-}silicate}$ of enstatite chondrites varies from -0.44‰ in Abee (impact EH4) to +0.16‰ in St.Marks (EH5) and correlate with the metamorphic temperature. This trend indicates a process of calcium redistribution from type 3 chondrites to the type 6 chondrites, driven by thermal metamorphism. The observed positive $\Delta^{44/40}Ca_{oldhamite\text{-}silicate}$ values in unequilibrated EH3 chondrites reflect kinetic Ca isotope fractionation between oldhamite and the nebular gas, providing evidence for the formation of oldhamite through condensation or interaction with the gas in the solar nebula.

Acknowledgement

We deeply thank Tahar Hammouda and two anonymous reviewers for constructive comments that greatly improved our manuscript. F. M. thanks the DIM ACAV+ (Domaine d'Interet Majeur, Astrophysique et Condition d'Apparition de la Vie) of the region Ile de France for providing part of the funding for the Nu Sapphire. F.M. acknowledges financial support from the Horizon ERC METAL (# 101001282). Parts of this work were supported by IPGP multidisciplinary program PARI. W.D. thanks the financial support of the Chinese Scholarship Council (CSC, No. 202006410008).

Data availability

Data are available through Zenodo at https://doi.org/10.5281/zenodo.10893913.

Appendix A. Supplementary Material

Two supplementary files are attached to this article. The first file is a spreadsheet and contains the elemental abundance of different parts of our leaching experiments (Table S1), the detailed modal calculation of Ca and REE fractionation of aubrite magma crystallization (Table S2), the Ca isotope composition of enstatite meteorites in literatures (Table S3), and metamorphic/equilibrium temperature of enstatite meteorites calculated by different thermometers from literatures (Table S4). The second supplementary file contains additional figures, including the REE patterns of different fractions of our leaching experiments and the results of our model calculation (Figure S1), and the correlation between $\Delta^{44/40}Ca_{oldhamite\text{-}silicate}$ and metamorphic/crystallization temperature determined by other thermometers (Figure S2).

References

Amsellem, E., Moynier, F., Pringle, E.A., Bouvier, A., Chen, H., Day, J.M.D., 2017. Testing the chondrule-rich accretion model for planetary embryos using calcium isotopes. *Earth Planet. Sci. Lett.* 469, 75-83.

Antonelli, M.A., Mittal, T., McCarthy, A., Tripoli, B., Watkins, J.M., DePaolo, D.J., 2019. Ca isotopes record rapid crystal growth in volcanic and subvolcanic systems. *Proc. Natl. Acad. Sci.* 116(41), 20315-20321.

Anzures, B.A., Parman, S.W., Milliken, R.E., Namur, O., Cartier, C., Wang, S., 2020. Effect of sulfur speciation on chemical and physical properties of very reduced mercurian melts. *Geochim. Cosmochim. Acta* 286, 1-18.

Barrat, J.-A., Bischoff, A., Zanda, B., 2023. Trace element redistributions during metamorphism of E-chondrites: Implications for reduced bodies and the Earth. *Geochim. Cosmochim. Acta* 356, 51-65.

Barrat, J.A., Zanda, B., Jambon, A., Bollinger, C., 2014. The lithophile trace elements in enstatite chondrites. *Geochim. Cosmochim. Acta* 128, 71-94.

Boyet, M., Carlson, R.W., 2007. A highly depleted moon or a non-magma ocean origin for the lunar crust? *Earth Planet. Sci. Lett.* 262(3-4), 505-516.

Boyet, M., Gannoun, A., 2013. Nucleosynthetic Nd isotope anomalies in primitive enstatite chondrites. *Geochim. Cosmochim. Acta* 121, 652-666.

Cartier, C., Wood, B.J., 2019. The Role of Reducing Conditions in Building Mercury. *Elements* 15(1), 39-45.

Chase, M., 1998. NIST-JANAF Thermochemical Tables, 4th Edition. American Institute of Physics.

Dai, W., Moynier, F., Fang, L., Siebert, J., 2023a. K-Ca dating and Ca isotope composition of the oldest Solar System lava, Erg Chech 002. *Geochem. Perspect. Lett.* 24, 33-37.

Dai, W., Moynier, F., Cui, M., Siebert, J., 2023b. Calcium isotopic composition of widely available

biological reference materials using collision cell (CC)-MC-ICP-MS. *J. Trace Elem. Miner.* 5, 100082.

Dai, W., Moynier, F., Paquet, M., Moureau, J., Debret, B., Siebert, J., Gerard, Y., Zhao, Y., 2022. Calcium isotope measurements using a collision cell (CC)-MC-ICP-MS. *Chem. Geol.* 590, 120688.

Dickinson, T.L., McCoy, T.J., 1997. Experimental rare-earth-element partitioning in oldhamite: Implications for the igneous origin of aubritic oldhamite. *Meteorit. Planet. Sci.* 32(3), 395-412.

Ebel, D.S., Binzel, R.P., Walker, R.M., Cameron, A.G.W., 2006. Condensation of Rocky Material in Astrophysical Environments, in: Lauretta, D.S., McSween, H.Y. (Eds.), *Meteorites and the Early Solar System II.* University of Arizona Press, pp. 253-278.

Feng, L., Zhou, L., Yang, L., Zhang, W., Wang, Q., Shuoyun, T., Hu, Z., 2018. A rapid and simple single-stage method for Ca separation from geological and biological samples for isotopic analysis by MC-ICP-MS. *J. Anal. At. Spectrom.* 33(3), 413-421.

Fitoussi, C., Bourdon, B., 2012. Silicon Isotope Evidence Against an Enstatite Chondrite Earth. *Science* 335(6075), 1477-1480.

Floss, C., Crozaz, G., 1993. Heterogeneous REE patterns in oldhamite from aubrites: Their nature and origin. *Geochim. Cosmochim. Acta* 57(16), 4039-4057.

Fogel, R., Weisberg, M., Prinz, M., 1996. The Solubility of CaS in Aubrite Silicate Melts, *Lunar Planet. Sci.* 27, 371–372.

Gannoun, A., Boyet, M., El Goresy, A., Devouard, B., 2011. REE and actinide microdistribution in Sahara 97072 and ALHA77295 EH3 chondrites: A combined cosmochemical and petrologic investigation. *Geochim. Cosmochim. Acta* 75(11), 3269-3289.

Hammouda, T., Boyet, M., Frossard, P., Cartier, C., 2022. The message of oldhamites from enstatite chondrites. *Prog. Earth Planet. Sci.* 9(1), 13.

He, Y., Wang, Y., Zhu, C., Huang, S., Li, S., 2017. Mass-Independent and Mass-Dependent Ca Isotopic Compositions of Thirteen Geological Reference Materials Measured by Thermal Ionisation Mass Spectrometry. *Geostand. Geoanal. Res.* 41(2), 283-302.

Horstmann, M., Humayun, M., Bischoff, A., 2014. Clues to the origin of metal in Almahata Sitta EL and EH chondrites and implications for primitive E chondrite thermal histories. *Geochim. Cosmochim. Acta* 140, 720-744.

Huang, F., Zhou, C., Wang, W., Kang, J., Wu, Z., 2019. First-principles calculations of equilibrium Ca isotope fractionation: Implications for oldhamite formation and evolution of lunar magma ocean. *Earth Planet. Sci. Lett.* 510, 153-160.

Huang, S.C., Jacobsen, S.B., 2017. Calcium isotopic compositions of chondrites. *Geochim. Cosmochim. Acta* 201, 364-376.

Huss, G.R., Lewis, R.S., 1994. Noble gases in presolar diamonds II: Component abundances reflect thermal processing. *Meteoritics* 29(6), 811-829.

Huss, G.R., Rubin, A.E., Grossman, J.N., 2006. Thermal Metamorphism in Chondrites, in: Lauretta, D.S., McSween, H.Y. (Eds.), *Meteorites and the Early Solar System II.* University of Arizona Press, pp. 567-586.

Inglis, E.C., Creech, J.B., Deng, Z., Moynier, F., 2018. High-precision zirconium stable isotope measurements of geological reference materials as measured by double-spike MC-ICPMS. *Chem. Geol.* 493, 544-552.

Ingrao, N.J., Hammouda, T., Boyet, M., Gaborieau, M., Moine, B.N., Vlastelic, I., Bouhifd, M.A.,

609 Devidal, J.L., Mathon, O., Testemale, D., Hazemann, J.L., Proux, O., 2019. Rare earth element
610 partitioning between sulphides and melt: Evidence for Yb^{2+} and Sm^{2+} in EH chondrites. *Geochim.*
611 *Cosmochim. Acta* 265, 182-197.
612 Javoy, M., 1995. The integral enstatite chondrite model of the Earth. *Geophys. Res. Lett.* 22(16), 2219-
613 2222.
614 Javoy, M., Kaminski, E., Guyot, F., Andrault, D., Sanloup, C., Moreira, M., Labrosse, S., Jambon, A.,
615 Agrinier, P., Davaille, A., Jaupart, C., 2010. The chemical composition of the Earth: Enstatite
616 chondrite models. *Earth Planet. Sci. Lett.* 293(3-4), 259-268.
617 Javoy, M., Pineau, F., Delorme, H., 1986. Carbon and nitrogen isotopes in the mantle. *Chem. Geol.*
618 57(1), 41-62.
619 Jordan, M.K., Tang, H., Kohl, I.E., Young, E.D., 2019. Iron isotope constraints on planetesimal core
620 formation in the early solar system. *Geochim. Cosmochim. Acta* 246, 461-477.
621 Kang, J.-T., Ionov, D.A., Liu, F., Zhang, C.-L., Golovin, A.V., Qin, L.-P., Zhang, Z.-F., Huang, F., 2017.
622 Calcium isotopic fractionation in mantle peridotites by melting and metasomatism and Ca isotope
623 composition of the Bulk Silicate Earth. *Earth Planet. Sci. Lett.* 474, 128-137.
624 Keil, K., 1989. Enstatite meteorites and their parent bodies*. *Meteoritics* 24(4), 195-208.
625 Li, M., Lei, Y., Feng, L., Wang, Z., Belshaw, N.S., Hu, Z., Liu, Y., Zhou, L., Chen, H., Chai, X., 2018.
626 High-precision Ca isotopic measurement using a large geometry high resolution MC-ICP-MS with
627 a dummy bucket. *J. Anal. At. Spectrom.* 33(10), 1707-1719.
628 Liu, F., Zhu, H.L., Li, X., Wang, G.Q., Zhang, Z.F., 2017. Calcium Isotopic Fractionation and
629 Compositions of Geochemical Reference Materials. *Geostand. Geoanal. Res.* 41(4), 675-688.
630 Lodders, K., 1996. Oldhamite in enstatite achondrites (Aubrites). *Proc. NIPR Symp. Antarct.*
631 *Meteorites* 9, 127-142.
632 Lodders, K., Fegley, B., 1993. Lanthanide and actinide chemistry at highCO/ ratios in the solar nebula.
633 *Earth Planet. Sci. Lett.* 117(1), 125-145.
634 Malavergne, V., Cordier, P., Righter, K., Brunet, F., Zanda, B., Addad, A., Smith, T., Bureau, H., Surblé,
635 S., Raepsaet, C., Charon, E., Hewins, R.H., 2014. How Mercury can be the most reduced
636 terrestrial planet and still store iron in its mantle. *Earth Planet. Sci. Lett.* 394, 186-197.
637 Mason, B., 1966. The enstatite chondrites. *Geochim. Cosmochim. Acta* 30(1), 23-39.
638 McCoy, T.J., Dickinson, T.L., Lofgren, G.E., 1999. Partial melting of the Indarch (EH4) meteorite: A
639 textural, chemical, and phase relations view of melting and melt migration. *Meteorit. Planet. Sci.*
640 34(5), 735-746.
641 Mougel, B., Moynier, F., Göpel, C., 2018. Chromium isotopic homogeneity between the Moon, the
642 Earth, and enstatite chondrites. *Earth Planet. Sci. Lett.* 481, 1-8.
643 Namur, O., Charlier, B., Holtz, F., Cartier, C., McCammon, C., 2016. Sulfur solubility in reduced mafic
644 silicate melts: Implications for the speciation and distribution of sulfur on Mercury. *Earth Planet.*
645 *Sci. Lett.* 448, 102-114.
646 Okada, A., Keil, K., Taylor, G.J., Newsom, H., 1988. Igneous History of the Aubrite Parent Asteroid:
647 Evidence from the Norton County Enstatite Achondrite. *Meteoritics* 23(1), 59-74.
648 Piani, L., Marrocchi, Y., Libourel, G., Tissandier, L., 2016. Magmatic sulfides in the porphyritic
649 chondrules of EH enstatite chondrites. *Geochim. Cosmochim. Acta* 195, 84-99.
650 Rubin, A.E., Huber, H., Wasson, J.T., 2009. Possible impact-induced refractory-lithophile
651 fractionations in EL chondrites. *Geochim. Cosmochim. Acta* 73(5), 1523-1537.
652 Rubin, A.E., Scott, W.R.D., 1997. Abee and related EH chondrite impact-melt breccias. *Geochim.*

653 *Cosmochim. Acta* 61(2), 425-435.
654 Russell, W.A., Papanastassiou, D.A., Tombrello, T.A., 1978. Ca isotope fractionation on the Earth and
655 other solar system materials. *Geochim. Cosmochim. Acta* 42(8), 1075-1090.
656 Schiller, M., Bizzarro, M., Fernandes, V.A., 2018. Isotopic evolution of the protoplanetary disk and the
657 building blocks of Earth and the Moon. *Nature* 555, 507.
658 Schiller, M., Paton, C., Bizzarro, M., 2012. Calcium isotope measurement by combined HR-MC-
659 ICPMS and TIMS. *J. Anal. At. Spectrom.* 27(1), 38-49.
660 Siebert, J., Malavergne, V., Guyot, F., Combes, R., Martinez, I., 2004. The behaviour of sulphur in
661 metal–silicate core segregation experiments under reducing conditions. *Physics of the Earth and*
662 *Planetary Interiors* 143-144, 433-443.
663 Simon, J.I., DePaolo, D.J., 2010. Stable calcium isotopic composition of meteorites and rocky planets.
664 *Earth Planet. Sci. Lett.* 289(3-4), 457-466.
665 Simon, J.I., DePaolo, D.J., Moynier, F., 2009. Calcium Isotope Composition of Meteorites, Earth, and
666 Mars. *Astrophys. J.* 702(1), 707-715.
667 Trieloff, M., Jessberger, E.K., Herrwerth, I., Hopp, J., Fiéni, C., Ghélis, M., Bourot-Denise, M., Pellas,
668 P., 2003. Structure and thermal history of the H-chondrite parent asteroid revealed by
669 thermochronometry. *Nature* 422(6931), 502-506.
670 Trinquier, A., Elliott, T., Ulfbeck, D., Coath, C., Krot, A.N., Bizzarro, M., 2009. Origin of
671 Nucleosynthetic Isotope Heterogeneity in the Solar Protoplanetary Disk. *Science* 324(5925), 374-
672 376.
673 Udry, A., Wilbur, Z.E., Rahib, R.R., McCubbin, F.M., Vander Kaaden, K.E., McCoy, T.J., Ziegler, K.,
674 Gross, J., DeFelice, C., Combs, L., Turrin, B.D., 2019. Reclassification of four aubrites as
675 enstatite chondrite impact melts: Potential geochemical analogs for Mercury. *Meteorit. Planet. Sci.*
676 54(4), 785-810.
677 Valdes, M.C., Moreira, M., Foriel, J., Moynier, F., 2014. The nature of Earth's building blocks as
678 revealed by calcium isotopes. *Earth Planet. Sci. Lett.* 394, 135-145.
679 Vander Kaaden, K.E., McCubbin, F.M., 2015. Exotic crust formation on Mercury: Consequences of a
680 shallow, FeO-poor mantle. *J. Geophys. Res. Planets* 120(2), 195-209.
681 Wadhwa, M., 2008. Redox Conditions on Small Bodies, the Moon and Mars. *Rev. Mineral. Geochem.*
682 68(1), 493-510.
683 Weisberg, M.K., Kimura, M., 2012. The unequilibrated enstatite chondrites. *Geochemistry* 72(2), 101-
684 115.
685 Weyrauch, M., Horstmann, M., Bischoff, A., 2018. Chemical variations of sulfides and metal in
686 enstatite chondrites—Introduction of a new classification scheme. *Meteorit. Planet. Sci.* 53(3),
687 394-415.
688 Wheelock, M.M., Keil, K., Floss, C., Taylor, G.J., Crozaz, G., 1994. REE geochemistry of oldhamite-
689 dominated clasts from the Norton County aubrite: Igneous origin of oldhamite. *Geochim.*
690 *Cosmochim. Acta* 58(1), 449-458.
691 Wohlers, A., Wood, B.J., 2015. A Mercury-like component of early Earth yields uranium in the core
692 and high mantle ^{142}Nd. *Nature* 520(7547), 337-340.
693 Wood, B.J., Kiseeva, E.S., Mirolo, F.J., 2014. Accretion and core formation: the effects of sulfur on
694 metal-silicate partition coefficients. *Geochim. Cosmochim. Acta* 145(0), 248-267.
695 Yokoyama, T., Misawa, K., Okano, O., Shih, C.-Y., Nyquist, L.E., Simon, J.I., Tappa, M.J., Yoneda, S.,
696 2017. Extreme early solar system chemical fractionation recorded by alkali-rich clasts contained

in ordinary chondrite breccias. *Earth Planet. Sci. Lett.* 458, 233-240.
Zhang, J., Dauphas, N., Davis, A.M., Leya, I., Fedkin, A., 2012. The proto-Earth as a significant source of lunar material. *Nat. Geosci.* 5(4), 251-255.
Zhang, Y., Sears, D.W.G., 1996. The thermometry of enstatite chondrites: A brief review and update. *Meteorit. Planet. Sci.* 31(5), 647-655.

Figure caption

Figure 1. Ca isotope composition of enstatite meteorites and leached oldhamite and residual fractions. The grey band represents the $\delta^{44/40}$Ca of the bulk silicate earth from Kang et al. (2017), 0.94 ± 0.05‰. The red bands represent the average $\delta^{44/40}$Ca (1.10 ± 0.06‰, 2SD) of enstatite chondrites estimated by EH and EL3 chondrites in this study. The Ca isotope composition of different enstatite meteorites reported in the literature are shown for comparison (Table S3, Huang and Jacobsen, 2017; Simon and DePaolo, 2010). For data measured by MC-ICP-MS, the $\delta^{44/40}$Ca value have been renormalized to Ca standard SRM 915a with -0.36 ε-unit anomalies on ^{40}Ca (Amsellem et al., 2017; Valdes et al., 2014).

Figure 2. (a) Leachate contribution to the Ca budget in different enstatite meteorites. (b) Contribution of six major elements to the bulk leachate budget of different enstatite meteorites. The detailed content of each leachate is listed in Table 2. (c) Plots of crystallization temperature for Norton County and metamorphic temperatures for enstatite chondrites versus Na/Ca ratio of their leachates in this study. The thermometer for estimating the metamorphic temperature of enstatite chondrites is from Zhang and Sears (1996). The estimation of equilibrium temperature of Norton County is from Lodders (1996) and Jordan et al. (2019). For samples without relative mineral data for calculation, the metamorphic temperature are estimated by average range of their metamorphic grades (Zhang and Sears, 1996).

Figure 3. Ca isotope composition of Abee (Impact melt breccia) meteorite.

Figure 4. Plots of the crystallization temperature for Norton County and metamorphic temperatures for enstatite chondrites versus $\Delta^{44/40}Ca_{oldhamite\text{-}silicate}$ values from meteorites in this study. One data from Valdes et al. (2014) is shown for comparison. The dashed lines are theoretical equations of equilibrium fractionation between oldhamite and other silicate minerals, including clinopyroxene (Cpx), orthopyroxene (enstatite, En) and plagioclase (anorthite, An) (Huang et al., 2019).

Figure 5. Modelled $\delta^{44/40}Ca$ of oldhamite-rich melt and differentiated silicate cumulates versus their relative REE distribution during aubritic magma crystallization. The $\delta^{44/40}Ca$ of starting material is 1.21‰ by mass balance calculation of our results. The REE distribution is calculated by the most abundant REE element, Ce, and normalized to CI abundance. Our measured data on single oldhamite phenocrysts, leachate and residual of Norton County are shown for comparison. The nature observation and model calculation agree well.

Figure 6. Schematic illustration of Ca isotope fractionation during highly reduced planetary embryos (Mercury and enstatite meteorite parent body). (a) metamorphism, (b) mantle melting, (c) magma ocean crystallization.

Table 1. Ca isotope composition of enstatite meteorites and relative leaching and Residual fractions in this study

Sample Name	Type	Note	K/Ca$_{mass}$	$\delta^{40/44}Ca$[1]	2sd	$\delta^{42/44}Ca$[1]	2sd	$\delta^{43/44}Ca$[1]	2sd	n	$\delta^{44/40}Ca_{SRM915a}$	$\delta^{44/40}Ca_{age\text{-}Corrected}$[2]	2sd	$\varepsilon^{40}Ca$	$\varepsilon^{40}Ca_0$[3]	2se
				‰		‰		‰			‰	‰				
Sahara 97096	EH3	Bulk rock	0.044	-0.34	0.06	-0.19	0.07	-0.09	0.06	8	1.06	1.12	0.06	0.48	-0.07	0.41
		replicate	0.044	-0.33	0.09	-0.19	0.06	-0.13	0.03	4	1.05	1.10	0.09	0.48	-0.07	0.51
		Residue	0.084	-0.28	0.08	-0.18	0.03	-0.05	0.07	7	1.00	1.11	0.08	0.77	-0.28	0.17
		Leachate	0.000	-0.49	0.05	-0.22	0.05	-0.12	0.02	4	1.21	1.21	0.05	-0.46	-0.46	0.34
		Calculated bulk										1.14	0.09		-0.27	0.23
Qingzhen	EH3	Bulk rock	0.087	-0.23	0.07	-0.15	0.07	-0.13	0.07	4	0.95	1.05	0.07	0.80	-0.29	0.44
		Residue	0.177	-0.07	0.05	-0.08	0.09	-0.15	0.16	4	0.79	1.01	0.05	1.00	-1.22	0.74
		Leachate	0.022	-0.39	0.07	-0.19	0.05	-0.12	0.13	6	1.11	1.14	0.07	-0.02	-0.29	0.70
		Calculated bulk										1.09	0.09		-0.60	0.62
NWA13299	EH3	Bulk rock	0.206	-0.13	0.09	-0.18	0.05	-0.10	0.08	4	0.85	1.11	0.09	2.34	-0.24	0.67
		Residue	0.320	0.08	0.08	-0.14	0.07	-0.13	0.13	3	0.64	1.04	0.08	3.66	-0.37	0.51
		Leachate	0.020	-0.39	0.01	-0.23	0.01	-0.08	0.03	3	1.11	1.13	0.01	0.72	0.47	0.11
		Calculated bulk										1.07	0.08		-0.05	0.52
Indarch	EH4	Bulk rock	0.076	-0.28	0.07	-0.18	0.08	-0.10	0.03	3	1.00	1.09	0.07	0.89	-0.06	0.55
		Residue	0.245	-0.13	0.06	-0.24	0.09	-0.05	0.09	4	0.85	1.16	0.06	3.58	0.51	0.70
		Leachate	0.003	-0.30	0.06	-0.20	0.06	-0.07	0.03	3	1.02	1.02	0.06	0.81	0.77	0.63
		Calculated bulk										1.09	0.09		0.41	0.49
St.Marks	EH5	Bulk rock	0.066	-0.34	0.04	-0.18	0.08	-0.09	0.13	4	1.06	1.15	0.04	0.21	-0.62	0.59
		Residue	0.283	-0.01	0.08	-0.13	0.05	-0.06	0.06	5	0.73	1.08	0.08	2.60	-0.95	0.25
		Leachate	0.004	-0.52	0.05	-0.22	0.04	-0.11	0.13	4	1.24	1.24	0.05	-0.70	-0.75	0.47
		Calculated bulk										1.19	0.09		-0.77	0.19
NWA12945	EH6	Bulk rock	0.099	-0.23	0.07	-0.12	0.05	-0.05	0.06	7	0.95	1.07	0.07	0.13	-1.11	0.22
		Residue	0.137	-0.32	0.04	-0.23	0.06	-0.11	0.08	6	1.04	1.22	0.04	1.44	-0.27	0.25
		Leachate	0.063	0.00	0.04	0.00	0.05	-0.01	0.07	4	0.72	0.80	0.04	0.02	-0.78	0.18

		Calculated bulk										1.00	0.06		-0.72	0.48
Abee	EH Impact-melt breccia	Bulk rock	0.089	-0.28	0.05	-0.16	0.08	-0.13	0.14	3	1.00	1.11	0.05	0.51	-0.61	0.15
		Residue	0.215	-0.43	0.05	-0.31	0.04	-0.08	0.09	5	1.15	1.42	0.05	1.95	-0.76	0.23
		Leachate	0.003	-0.25	0.00	-0.11	0.03	-0.03	0.11	2	0.97	0.98	0.00	-0.24	-0.28	0.27
		Calculated bulk										1.15	0.05		-0.55	0.28
MAC02837	EL3	Bulk rock	0.045	-0.30	0.04	-0.18	0.01	-0.10	0.14	6	1.02	1.08	0.04	0.76	0.19	0.06
		Residue	0.083	-0.251	0.05	-0.19	0.03	-0.11	0.14	6	0.97	1.08	0.05	1.39	0.35	0.12
		Leachate	0.002	-0.35	0.06	-0.19	0.09	-0.11	0.09	9	1.07	1.07	0.06	0.32	0.29	0.55
		Calculated bulk										1.07	0.08		0.28	0.31
Ufana	EL6	Bulk rock	0.064	-0.41	0.07	-0.22	0.09	-0.12	0.09	6	1.13	1.21	0.07	0.37	-0.43	0.45
		Residue	0.086	-0.45	0.02	-0.24	0.05	-0.11	0.08	6	1.17	1.28	0.02	0.31	-0.77	0.35
		Leachate	0.001	-0.43	0.05	-0.15	0.06	-0.09	0.06	4	1.15	1.15	0.05	-1.20	-1.22	0.59
		Calculated bulk										1.24	0.06		-0.81	0.45
Pillistfer	EL6	Bulk rock	0.065	-0.43	0.07	-0.23	0.09	-0.06	0.07	4	1.15	1.24	0.07	0.33	-0.49	0.63
		Residue	0.082	-0.49	0.09	-0.26	0.04	-0.13	0.07	4	1.21	1.31	0.09	0.38	-0.65	0.67
		replicate	0.082	-0.53	0.06	-0.27	0.02	-0.16	0.08	4	1.25	1.35	0.06	0.37	-0.66	0.28
		Leachate	0.004	-0.31	0.06	-0.12	0.03	-0.07	0.09	5	1.03	1.04	0.06	-0.66	-0.71	0.24
		Calculated bulk										1.28	0.09		-0.63	0.11
Hvittis	EL6	Bulk rock	0.075	-0.35	0.10	-0.13	0.07	-0.14	0.10	4	1.07	1.16	0.10	-0.84	-1.78	0.27
		replicate	0.075	-0.40	0.04	-0.20	0.03	-0.04	0.05	4	1.12	1.22	0.04	0.05	-0.89	0.37
		Residue	0.092	-0.35	0.07	-0.13	0.06	-0.10	0.05	5	1.07	1.19	0.07	-0.85	-2.01	0.27
		replicate	0.092	-0.37	0.07	-0.24	0.04	0.00	0.09	3	1.09	1.21	0.07	1.15	0.00	0.60
		Leachate	0.012	-0.32	0.05	-0.12	0.02	-0.11	0.16	3	1.04	1.06	0.05	-0.76	-0.91	0.34
		Calculated bulk										1.18	0.08		-0.60	0.60
Norton County	Aubrite	Bulk rock	0.004	-0.40	0.05	-0.21	0.05	-0.11	0.05	4	1.12	1.12	0.05	0.38	0.33	0.41
		Residue	0.006	-0.54	0.07	-0.24	0.06	-0.14	0.06	7	1.26	1.27	0.07	-0.40	-0.47	0.33
		Leachate	0.003	-0.24	0.06	-0.12	0.08	-0.04	0.04	4	0.96	0.96	0.06	0.03	-0.01	0.71

	Single oldhamite 1	0.001	-0.11	0.03	-0.06	0.05	0.00	0.07	4	0.83	0.83	0.03	0.05	0.04	0.51
	Single oldhamite 2	0.000	-0.08	0.05	-0.01	0.03	0.01	0.04	7	0.80	0.80	0.05	-0.55	-0.55	0.29
	replicate	0.000	-0.10	0.09	-0.01	0.07	0.00	0.06	3	0.82	0.82	0.09	-0.80	-0.80	0.39
	Calculated bulk										1.21	0.09		-0.05	0.46
Reference materials															
NASS-7	Seawater		-1.20	0.08	-0.58	0.07	-0.28	0.11	20		1.92	0.08	-0.16		0.27
GSP-2	Granodiorite		0.44	0.08	0.00	0.09	0.03	0.05	5		0.71	0.08	4.36		0.49

1: The Ca isotope ratios are relative to SRM 915b.

2. For Hvittis, replicate measurements with higher precision are used for discussion in this study.

3. $\varepsilon^{40}Ca_0$ is calculated after correction of the radioactive decay of ^{40}K using the age of the samples around 4565 Ma.

Table 2. Mass and elemental budget of leachates from different enstatite meteorites

Sample name	Leach/WR	Old/WR	Old/Leach	Leach-Ca/WR	Leach-Ce/WR	Major elements content in leachate	Na	Mg	K	Ca	Mn	Fe
	wt. %	wt. %	wt. %	wt. %	wt. %		wt. %	wt. %	wt. %	wt. %	wt. %	wt. %
Sahara 97096	1.1%	0.6%	53.2%	32.8%	1.9%		28.7%	9.9%	0.0%	49.5%	0.3%	10.0%
Qingzhen	1.4%	0.9%	61.7%	58.0%	3.8%		12.3%	10.8%	1.3%	58.1%	0.4%	16.7%
NWA13299	1.0%	0.5%	51.6%	35.7%	2.8%		26.1%	7.8%	1.3%	48.0%	0.3%	16.2%
Indarch	3.3%	2.0%	58.9%	68.5%	1.1%		9.2%	26.7%	0.2%	59.1%	0.2%	4.5%
St.Marks	0.7%	0.6%	82.2%	65.9%	1.8%		3.0%	14.3%	0.4%	81.0%	0.5%	0.5%
NWA12945	1.0%	0.8%	85.5%	51.8%	1.8%		1.5%	5.0%	5.1%	80.7%	2.2%	5.3%
Abee	1.1%	0.9%	81.7%	61.0%	2.2%		7.5%	2.3%	0.5%	75.2%	0.3%	13.6%
MAC02837	1.4%	1.3%	93.4%	42.5%	1.9%		1.1%	4.2%	0.2%	90.3%	1.4%	2.9%
Ufana	0.5%	0.4%	82.6%	30.2%	8.2%		1.7%	3.8%	0.6%	76.7%	0.5%	15.7%
Pillistfer	0.3%	0.3%	100.0%	25.1%	0.7%		1.9%	1.0%	0.6%	93.4%	0.1%	2.8%
Hvittis	0.5%	0.4%	78.2%	22.8%	2.1%		4.4%	7.3%	0.9%	74.1%	0.4%	11.9%
Norton County	1.4%	0.8%	57.4%	20.6%	6.2%		0.6%	35.8%	0.2%	59.2%	1.8%	1.1%

Detailed information on chemical composition of leachate and relative residual can be found in Table S1. The chemical composition of leachate shown in this table are calculated by normalizing the total mass of six major elements to 100%. Leach: leachate; WR: bulk meteorite; Old: oldhamite.

Figure 1

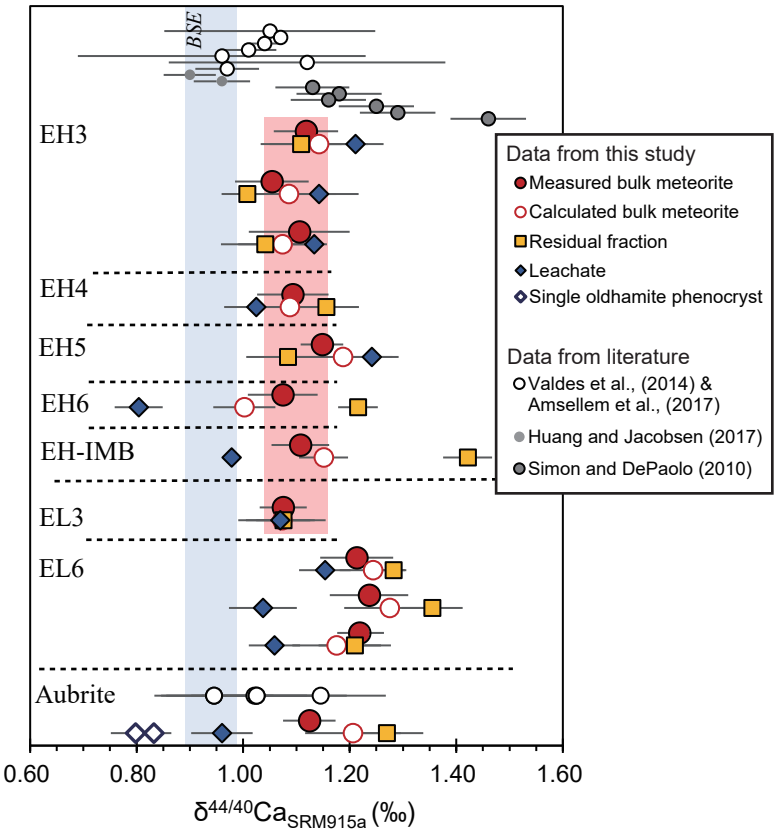
BSE
EH3
EH4
EH5
EH6
EH-IMB
EL3
EL6
Aubrite
0.60
0.80
1.00
1.20
1.40
1.60
δ44/40CaSRM915a (‰)
Data from this study
Measured bulk meteorite
Calculated bulk meteorite
Residual fraction
Leachate
Single oldhamite phenocryst
Data from literature
Valdes et al., (2014) & Amsellem et al., (2017)
Huang and Jacobsen (2017)
Simon and DePaolo (2010)

Figure 2

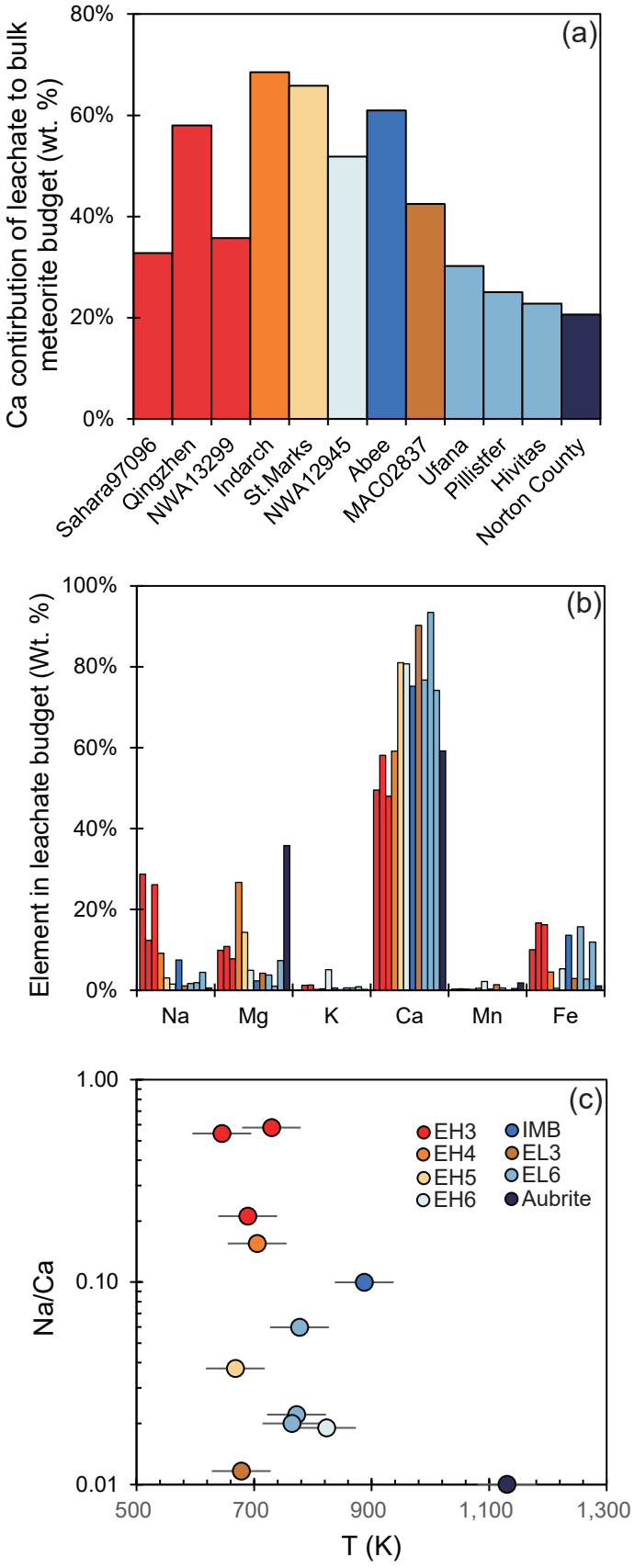
(a)
Ca contirbution of leachate to bulk meteorite budget (wt. %)
80%
60%
40%
20%
0%
Sahara97096
Qingzhen
NWA13299
Indarch
St.Marks
NWA12945
Abee
MAC02837
Ufana
Pillistfer
Hivitas
Norton County
(b)
Element in leachate budget (Wt. %)
100%
80%
60%
40%
20%
0%
Na
Mg
K
Ca
Mn
Fe
(c)
Na/Ca
1.00
0.10
0.01
EH3
EH4
EH5
EH6
IMB
EL3
EL6
Aubrite
500
700
900
1,100
1,300
T (K)

Figure 3

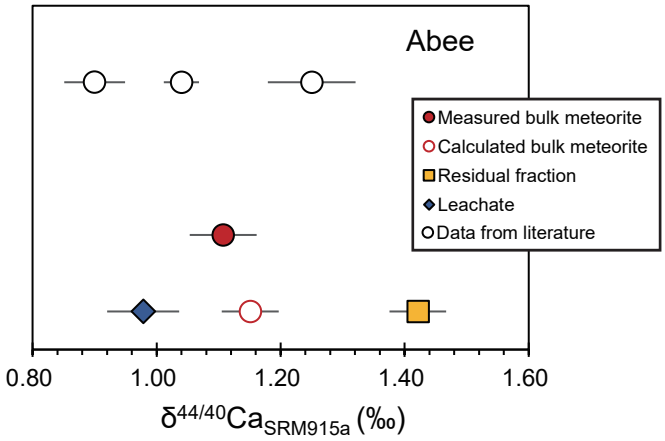
Abee
Measured bulk meteorite
Calculated bulk meteorite
Residual fraction
Leachate
Data from literature
0.80
1.00
1.20
1.40
1.60
δ44/40CaSRM915a (‰)

Figure 4

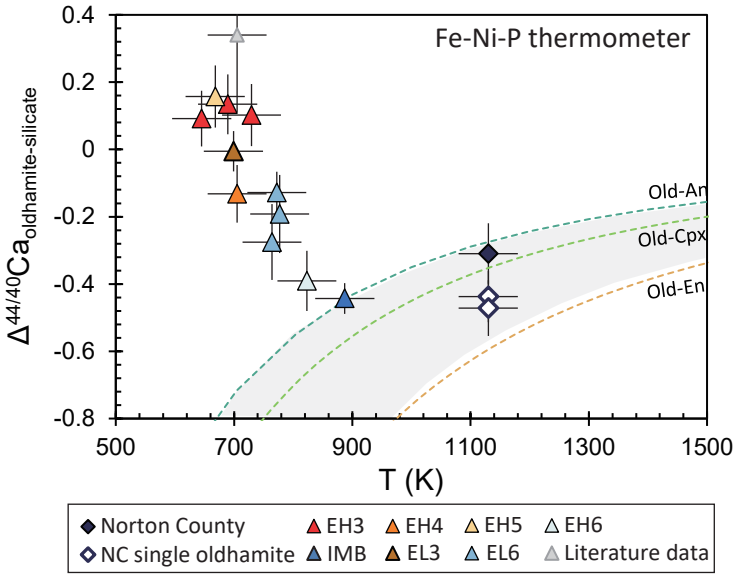
Fe-Ni-P thermometer
$\Delta^{44/40}Ca_{oldhamite\text{-}silicate}$
0.4
0.2
0
-0.2
-0.4
-0.6
-0.8
500
700
900
1100
1300
1500
T (K)
Old-Ar
Old-Cpx
Old-En
Norton County
NC single oldhamite
EH3
IMB
EH4
EL3
EH5
EL6
EH6
Literature data

Figure 5

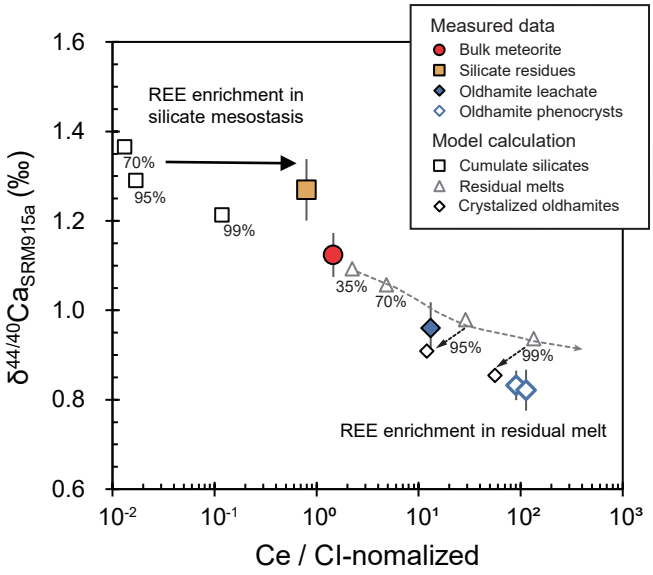
Measured data
Bulk meteorite
Silicate residues
Oldhamite leachate
Oldhamite phenocrysts
Model calculation
Cumulate silicates
Residual melts
Crystalized oldhamites
REE enrichment in
silicate mesostasis
70%
95%
99%
35%
70%
95%
99%
REE enrichment in residual melt
1.6
1.4
1.2
1.0
0.8
0.6
δ44/40CaSRM915a (‰)
10-2
10-1
10⁰
10¹
10²
10³
Ce / CI-nomalized

Figure 6

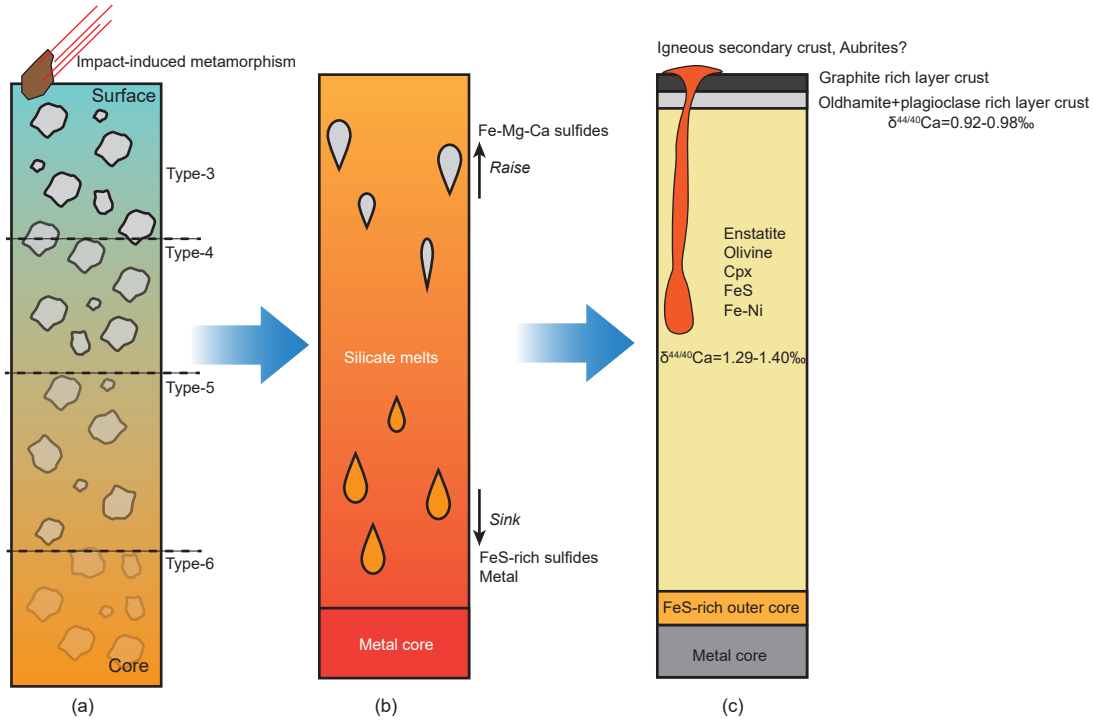
Impact-induced metamorphism
Surface
Type-3
Type-4
Type-5
Type-6
Core
(a)
Fe-Mg-Ca sulfides
Raise
Silicate melts
Sink
FeS-rich sulfides
Metal
Metal core
(b)
Igneous secondary crust, Aubrites?
Graphite rich layer crust
Oldhamite+plagioclase rich layer crust
δ44/40Ca=0.92-0.98‰
Enstatite
Olivine
Cpx
FeS
Fe-Ni
δ44/40Ca=1.29-1.40‰
FeS-rich outer core
Metal core
(c)